International Journal of Fluid Machinery and Systems
Vol. 7, No. 3, July-September 2014
DOI: http://dx.doi.org/10.5293/IJFMS.2014.7.3.110
ISSN (Online): 1882-9554

Original Paper

Surge Phenomena Analytically Predicted in a Multi-stage Axial Flow Compressor System in the Reduced-Speed Zone

Nobuyuki Yamaguchi[1]

[1]Meisei University (retired)
2-1-25, Akanedai, Aoba-ku, Yokohama-shi, 227-0066, JAPAN,
yamaguchi_nandm@hb.tp1.jp

Abstract

Surge phenomena in the zone of reduced speeds in a system of a nine-stage axial flow compressor coupled with ducts were studied analytically by use of a surge transient simulation code. Main results are as follows. (1) Expansion of apparently stable, non-surge working area of the pressure vs. flow field beyond the initial stage-stall line was predicted by the code in the lower speed region. The area proved analytically to be caused by significantly mismatched stage- working conditions, particularly with the front stages deep in the rotating stall branch of the characteristics, as was already known in situ and in steady-state calculations also. (2) Surge frequencies were found to increase for decreasing compressor speeds as far as the particular compressor system was concerned. (3) The tendency was found to be explained by a newly introduced volume-modified reduced surge frequency. It suggests that the surge frequency is related intimately with the process of emptying and filling of air into the delivery volume. (4) The upstream range of movement of the fluid mass having once passed through the compressor in surge was found to reduce toward the lower speeds, which could have caused additionally the increase in surge frequency. (5) The concept of the volume- modified reduced surge frequency was able to explain, though qualitatively at present, the behaviors of the area- pressure ratio parameter for the stall stagnation boundary proposed earlier by the author.

Keywords: Fluid Machine, Compressor, Surge, Analytical Simulation, Transient Flow, Fluid Dynamics

1. Introduction

In gas turbines, jet engines, and industrial compressor plants, compressor surges are often unavoidable. High pressure ratio compressors could happen to stall or surge deeply for changes in the overall pressure ratios and in the reduced speeds, for example, during abrupt load changes, start-ups or shut-downs, because of possible sudden excursions and/or mismatching of stage working conditions among the stages. In addition to these deep surges, in some conditions, so-called stall stagnations could occur, where the compressor falls into the rotating stall zone, tending difficult to recover to sound region. Thus the surge phenomena have been paid attention to from the aspect of operational safety and for countermeasures. In these situations, compressor speeds could have significant effects on the surge phenomena.

Compressor surge phenomena have often been studied analytically by relatively simple methods similar to ones on low-speed and low-pressure-ratio fans. Although some basic and qualitative explanations could be obtained about the surge, it was often difficult in the situation of high-pressure-ratio compressors to describe reasonably the violent transient behaviors of pressure and flow and to predict the quantitative features of the behaviors. At the same time, it is often difficult to conduct detailed and systematic experiments on surge in conditions of large-scale and high-pressure ratio compressors and/or plants because of several limitations mainly from the aspect of safety. Consequently, the very few experimental surge data obtained so far could be very valuable. They, however, could often be fragmentary in pieces and bits condition. In the situation, it will be important to clarify the whole picture of the phenomena on the basis of the few pieces of experimental information supported by analytical ones gained by some reliable simulation methods using appropriate data

Received July 27 2013; revised Decmber 29 2013; accepted for publication January 3 2014: Review conducted by Prof. Guang Xi. (Paper number O13028C)
Corresponding author: Nobuyuki Yamaguchi, yamaguchi_nandm@tk2.so-net.ne.jp

on stage characteristics and flow-path properties, and operating conditions, etc. For the purpose, the author has been developing a simulation code about surge transient phenomena (SRGTRAN, Yamaguchi [1]).

In the context, the author has analyzed by use of SRGTRAN the surge situation in a nine- stage axial flow compressor coupled with suction and delivery ducts over a range of compressor speeds, particularly in the lower speed region. The results show some interesting features for the changes in the compressor speeds, which suggest the complicated nature of the surge phenomena affected by various effects, such as stage mismatching conditions, acoustical resonance effects, flow convection effects, oscillation modes in the whole flow-path system, etc. The author would like to describe them for future reference, although corresponding data by experiments or actual machines are not available at present.

2. Analysis Procedure (SRGTRAN)

The simulation code, SRGTRAN, the details of which can be found in Yamaguchi [1], conducts analyses in space-time coordinate (x, t). The compressor flow-path is made up of a series of control volumes corresponding to respective stages in which equations of conservation of mass, momentum and energy are solved by the two-stage Lax-Wendroff method. The duct flow-paths are divided into a suitable number of control volumes (CVs) in which the method of characteristics is applied. Within the present formulation, it assumes the phenomena only in the axial direction and neglects the effects of circumferential components and the rotating stall phenomena as very small.

Time t is expressed as follows;

$$t=k\Delta t \qquad (1)$$

Here, Δt is the time step determined to satisfy the Courant-Friedrichs-Lewy condition. k means an integer variable showing time where k=0 means the starting time of the transient analysis.

The following relation is assumed to describe approximately the motion of the flow through the valve passage having a valve opening area Av and an equivalent length ΔLv (Yamaguchi [1, 3]).

$$\Delta L_V \frac{dW_V}{dt} = A_V (p_1 - p_2) - \frac{\beta_V}{\alpha_V} \frac{W_V^2}{\rho_1 A_V} \qquad (2)$$

Here, αv and βv are a valve flow coefficient and an adjusting coefficient, respectively. The inertia length of the valve flow passage is assumed to be given by;

$$\Delta Lv = \varepsilon v \sqrt{Av} \qquad (3)$$

Here, εv is an empirical adjusting factor.

Following values were assumed temporarily for the present analyses;

$$\alpha v = 1, \quad \beta v = 1, \quad \varepsilon v = 1 \qquad (4)$$

The initial valve opening area Avo is given by assuming that d Wv/dt is zero in Eq. (2) at the time when a responsible stage reaches first its stage-stalling point in the initial steady-state calculation. Then the transient analysis is started with the valve area being gradually throttled further to a final specified area Av given by the following relation.

$$Av = Av_0 (1 + Vcrat) \qquad (5)$$

Here, $Vcrat$ means a changing rate. After the final area is reached, it is kept constant. The following ratio gives the final valve area ratio.

$$Av/Avo \qquad (6)$$

3. Compressor and ducts for study

The compressor for study, whose main numerical figures are given in **Table 1,** is a nine stage axial flow compressor having a constant-hub annulus configuration with design conditions of overall pressure ratio 3.88 at 11300 rpm for the suction temperature 288.2 K. The compressor has repeated stages designed with the same design flow and pressure coefficients having approximately 50 % reaction degree. The stages have rather low relative inflow Mach numbers at the rotor tips.

Table 1 Compressor Dimensions

Type	Axial Flow Compressor
Stages	9
Tip and hub diameter for the first stage *Dt1 and Dh* (m)	0.508 0.356
Design speed (rpm)	11300
Design flow (m^3/s)	11.5
Design pressure ratio	3.82 (288.2 K)
Conditions for analysis	
RPM for analysis (approx. %design speed)	12400－6780 (110-60%)
Suction temperature	313.2 (K)
Stage characteristics	Identical for all stages

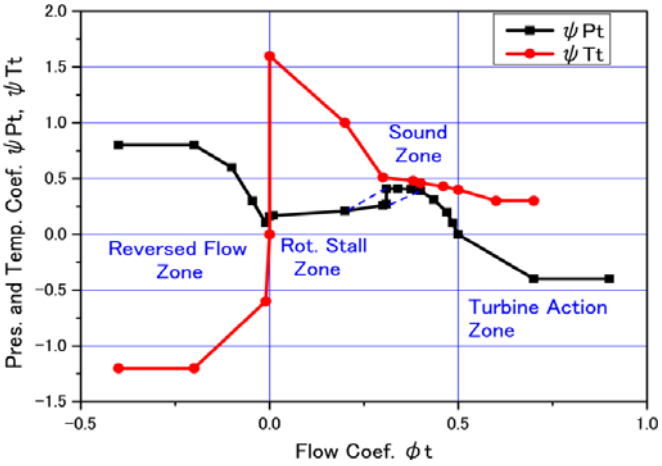

Fig. 1 Wide–range stage characteristics assumed for the compressor stages

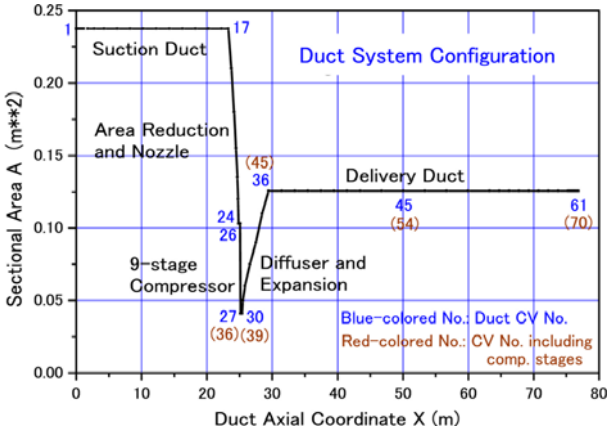

Fig. 2 Distribution of the flow-path sectional area against the duct axial coordinate and the control volume numbers

The surge analyses were conducted for the suction condition of 313.2 K and 101.3 kPa and for the 110-60 % design speed.

The employed stage characteristics is shown in **Fig. 1**, which is required to cover a wide range from the turbine-action zone to the reversed flow condition. The characteristics were constructed in reference to several literature (for example, Day, Greitzer, and Cumpsty [4], Gamache and Greitzer [5] , Greitzer [6], etc.).

Stage working conditions are estimated on the steady-state stage characteristics through the following parameters.

Flow coefficient:

$$\phi_t = u_m / u_t \tag{7}$$

Pressure coefficient:

$$\psi_{Pt} = \frac{C_P T_{T1}\left[\left(P_{T2}/P_{T1}\right)^{\{(\kappa-1)/\kappa\}} - 1\right]}{(1/2)u_t^{\,2}} \tag{8}$$

Temperature coefficient:

$$\psi_{Tt} = C_P\left(T_{T2} - T_{T1}\right)/(1/2)u_t^{\,2} \tag{9}$$

Here, u_m: annulus-averaged axial flow velocity, u_t: compressor tip peripheral speed of the first stage (reference speed), P_{T1} and T_{T1}: total pressure and temperature at the stage inlet, respectively, P_{T2} and T_{T2}: total pressure and temperature at the stage exit, respectively, and κ : ratio of specific heats.

Table 2 Time step for each compressor speed

rpm	Δt (s/div)
12400	1.357×10^{-5}
11300	1.404×10^{-5}
10170	1.449×10^{-5}
9040	1.484×10^{-5}
7910	1.471×10^{-5}
6780	1.491×10^{-5}

The stage characteristics were assumed to have an abrupt stall behavior as shown in **Fig. 1** because of the rather high load nature and the assumed relatively high hub-to-tip radius ratio. Because of the repeated stage configuration, each stage could reasonably be assumed to have the same characteristics. Influences of changes in the compressor rotational speeds on the normalized stage characteristics were assumed to be negligible within the range of this study since the relative inflow Mach numbers at the rotor inlet are relatively low. The identical characteristics were assumed for all the compressor speeds.

Axial distributions of stage blockage factors were kept the same for all the compressor speeds.

The suction duct has an open atmospheric inlet and a valve is mounted at the end of the delivery duct. Pipe frictions are specified as the friction factor of 0.02 but the most of the pressure losses are caused by the exit valve in this particular case. **Figure 2** shows the distribution of the duct sectional area A against the x coordinate with x=0 for the inlet of the suction duct. The numerical figures attached show the CV numbers of the control volumes (CV) constituting the flow-path where No. 1 is the inlet of the duct and No. 61 the exit. The compressor lies between 26 and 27. The numbers in ( ) are those including the compressor stage CVs, which are employed in the contour maps on flow conditions (**Fig.10**). The axial length of the compressor is seen to be very short compared with the whole duct length.

Table 2 shows the values of time step Δt employed in Eq. (1).

4. Surge Loops Changing with Compressor Speeds

Figure 3 shows surge loops of pressure vs. mass flow at the compressor exit for changes in the compressor speed. These performances were evaluated with the exit valve area ratio *Av/Avo* of 0.9 for 12400-10170 rpm (110-90% design speed), 0.8 for 9040 rpm (80%), 0.5 for 7910 rpm (70%), and 0.3 for 6780 rpm (60%). For the lower speeds, only such narrow valve areas could have forced the compressor into deep surge.

For each speed, the nearly vertical line in the large flow side is the near-steady-state characteristics, at whose top stalling occurs and a surge cycle is initiated. The dotted curve connecting the top points shoes the steady-state stall or surge line. After the stalling, the surge locus tends to jump onto the negative flow branch, along which the pressure drops, and jumps back to the positive flow zone, thus describing a loop. The surge loops for respective speeds, though different in size, are seen to show relatively similar behaviors.

Below 80% design speed (9040, 7910, and 6780rpm), the compressor stalls lightly and recovers instantaneously to some larger mass flow point, and rises to a pressure level corresponding to the exit valve area. Further throttling causes the pressure to rise further and, finally at some smaller valve area, results in a deep surge. **Figure 4** shows the low-speed surge loops in an expanded fashion. The shaded zone named "Rotating

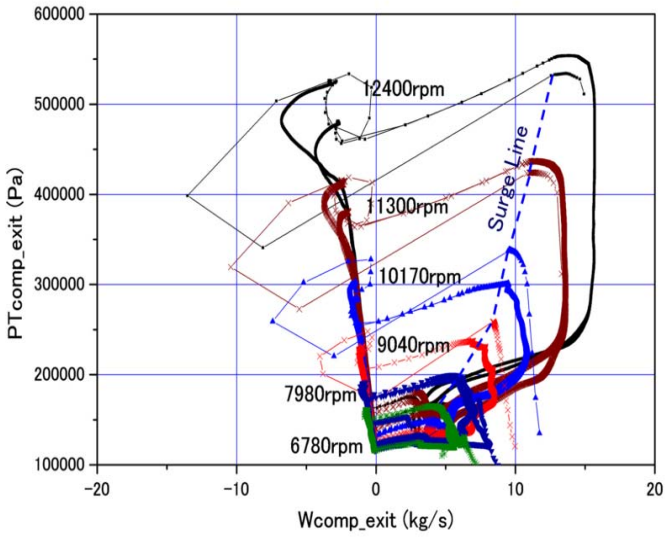

Fig. 3 Surge loops at the compressor exit location changing for different compressor speeds with the exit valve opening *Av/Avo* kept at 0.9 for 12400-10170 rpm, 0.8 at 9040 rpm, 0.5 at 7980 rpm, and 0.3 at 6780 rpm, respectively

Stall Zone" indicates the apparently stable, non-deep-surge area thus extended from the steady-state stage-stall line. In the zone, however, one or more front stages are observed to be working on the trotating stall branch of the stage characteristics, as shown later in **Fig.5**. Here, it is to be noted in this report that the occurrences of rotating stalls are judged by the stage working position located within the rotating stall branch of the characteristics shown in **Fig. 1**.

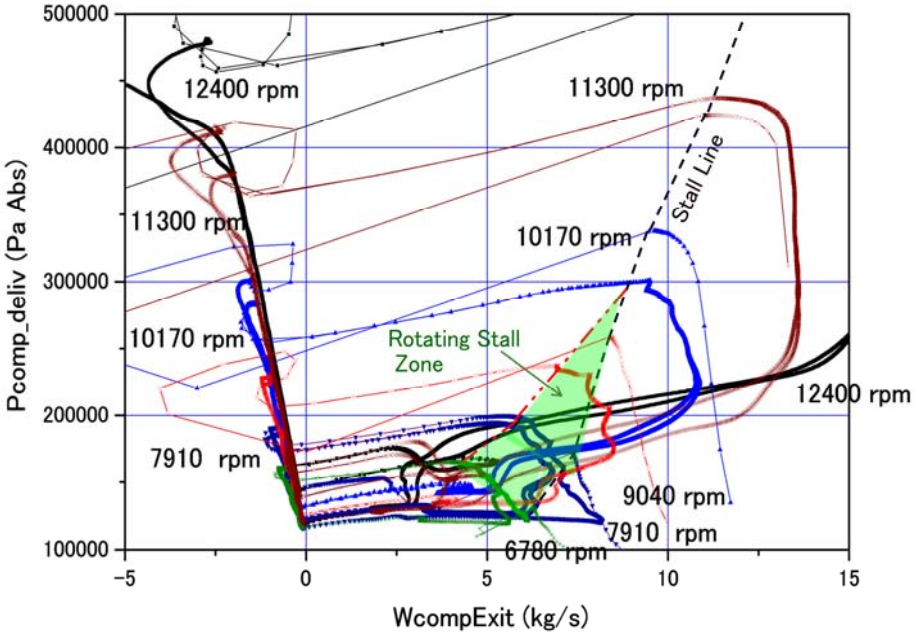

Fig. 4 Expanded view of the lower speed zone, showing appearance of a rotating stall zone toward the lower speed range in the compressor speed map

5. Situation into Deep Surge at a Reduced Speed

Figure 5 shows changes in the behaviors of pressure vs. mass flow at 6780 rpm resulted from throttling of the valve as an example of the low-speed surge loops shown in **Fig. 4**. At the valve area for the initial stage stall ing, i.e., *Av/Avo*=1 (**Fig. 5(a)**), a phenomenon of lightly stalling occurs, but immediately after that it recovers and settles to near below the initial stalling condition. At further throttled valve areas, *Av/Avo*=0.5 and 0.4 (**Fig. 5(b) and (c)**), they, having followed a similar process, settle to apparently stable higher pressure point. At further throttled valve condition, *Av/Avo*=0.3 (**Fig. 5(d)**), the pressure rises toward the highest pressure point, then stalls and breaks into deep surge cycles. These figures are superposed in **Fig. 5(e)**, which shows the process of surging in the course of throttling the exit valve at 6780 rpm. For the valve area ratio *Av/Avo* greater than 0.3, the pressure-flow slope is seen to be negative, meaning apparent global stability.

Figure 6 shows working conditions of each stage at 6780 rpm for the valve area ratio *Av/Avo*=1 (**Fig. 6(a)**), 0.4 (**Fig. 6(b)**), and 0.3 (**Fig. 6(c)**); flow coefficient ϕ_t in the top, and pressure coefficient ϕ_{Pt} in the bottom. Numerical numbers attached to the curves in **Fig. 6** indicate the stage number.

Figure 6(a) shows the condition for *Av/Avo*=1, where both flow coefficients ϕ_t and pressure coefficients ϕ_{Pt} do not move temporarily. At such a low-speed off-design condition, the stage-wise matching of the stage working conditions tend to deviate much from the designed one, resulting in deep-stalled front stages and in-turbine-action rear stages. As a global condition of the compressor, the negative slope of the pressure-flow field tends to be maintained, i.e., seemingly stable. However, the front stages are staying in the rotating-stall branch of the stage characteristics.

Figure 6(b) shows the condition for *Av/Avo*=0.4, where the valve is being throttled to 40% of the initial one in the time until *k* of 50000, and is kept constant after that. In the situation, all stage flow coefficients tend to decrease and the rear stage pressure coefficients increase from negative levels, but each settles at some insufficient level after reaching at a ceiling. These behaviors are similar to those predicted in the steady-state process near low-speed stalling. After all, the compressor results in a state of global stability.

Figure 6(c) shows the condition for *Av/Avo*=0.3, where the valve manipulation is similar to the above. The stage conditions follow a similar process as above until time *k* of 50000, but the exit pressure keeps increasing; correspondingly, rear stage flow coefficients keep decreasing and the pressure coefficients increasing until reaching the stalling condition. Around *k* of 70000, the compressor falls finally into global instability, i.e., deep surge, which is corresponding to the deep surge cycle shown in **Fig. 5(e)**.

Within the extended zone covering from the stage-stalling point for *Av/Avo*=1 to before the surge initiation for *Av/Avo*=0.3, the front stages are staying on the rotating stall branch of the stage characteristics. The situation is extremely dangerous since the compressor rotor and stator blades could be excited possibly to resonant vibration by relative movements of the stall cells.

Figure 7 shows oscillograms at the compressor exit of the mass flow (bottom) and the pressure (top) in deep surge condition for 100, 80, 60% design speed. For the higher speeds (**Fig. 7(c)**, 11300rpm, *Av/Avo*=0.9)), immediately after the initial stalling, the compressor pressure and mass flow drop steeply and break into deep surges. For the lower speed (**Fig. 7(a)**, 6780 rpm, *Av/Avo*=0.3), with the valve area being throttled gradually from the initial one, the mass flow reduces gradually and the pressure increases to the peak level around time *k* of 80000. After that, both the mass flow and the pressure drop steeply and break into a deep surge. The time is estimated by Eq. (1) and the time step Δt given in **Table 2**.

Details of the surge wave configurations, for example, sharpness of the pressure peaks, contents of higher order components in the bottom zones of the pressure and the mass flow, rising-edge behaviors of the mass flow recovery, etc., are seen to change in a delicate manner depending on the compressor speeds, possibly affected by many macroscopic and microscopic phenomena involved in the process. It would be difficult but necessary to figure out the complicated situations to understand the real surge phenomena.

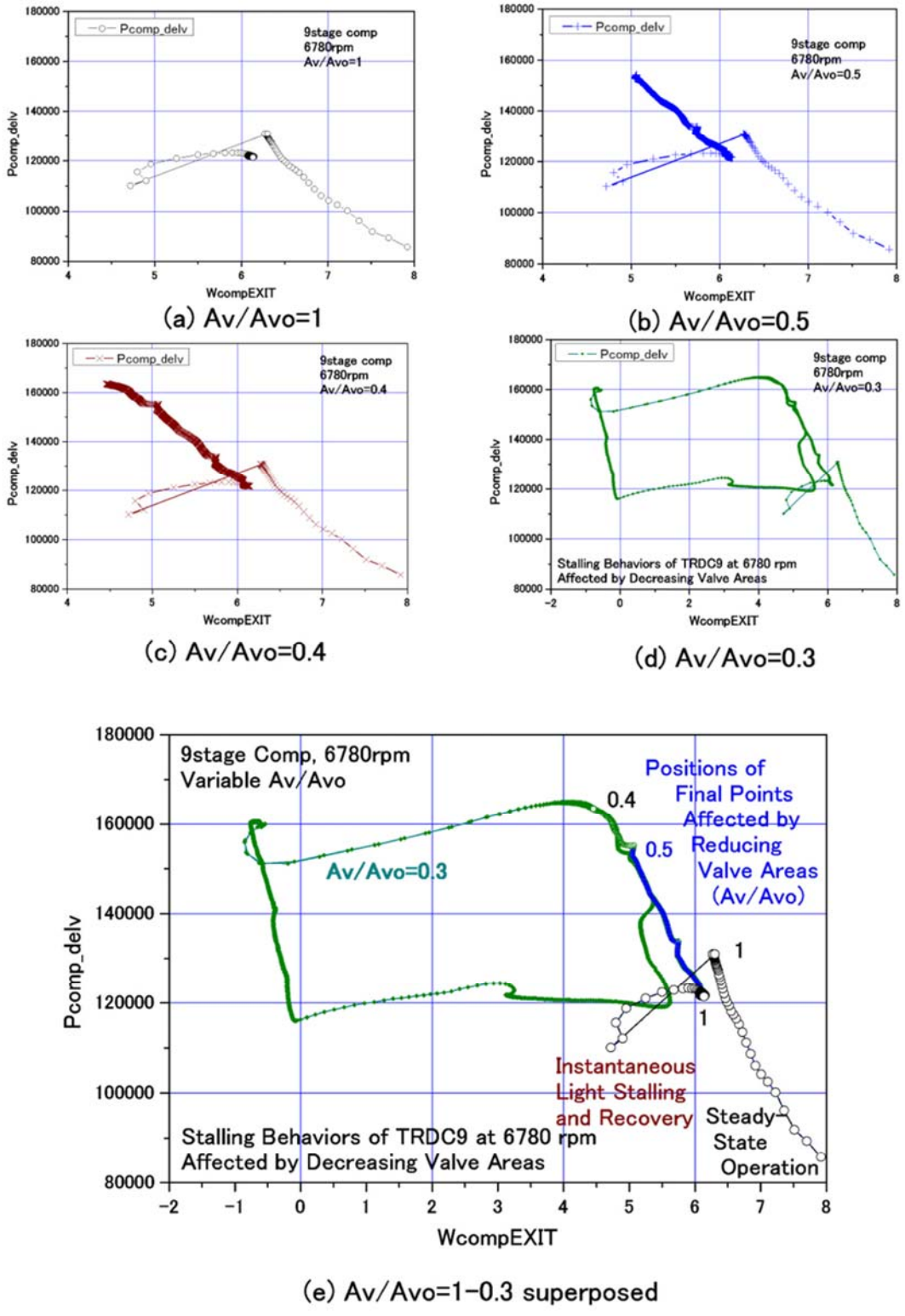

Fig. 5 Changing surge loops affected by relative valve openings *Av/Avo* at 6780 rpm. Fig.5(e) shows the resulting process into the situation of a deep surge condition when fully throttled.

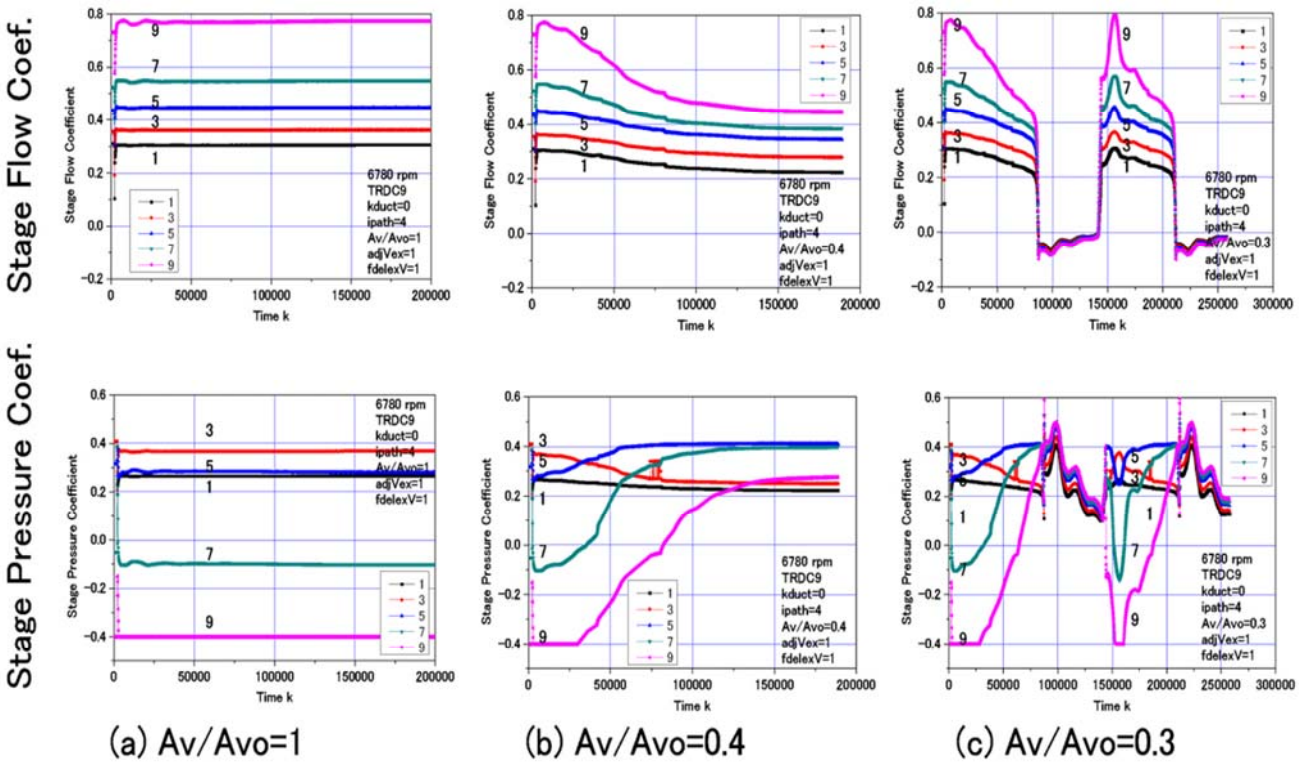

Fig. 6 Changes in the stage operating flow coefficients (top figures) and pressure coefficients (bottom figures) at 6780rpm affected by closing the exit valve opening.

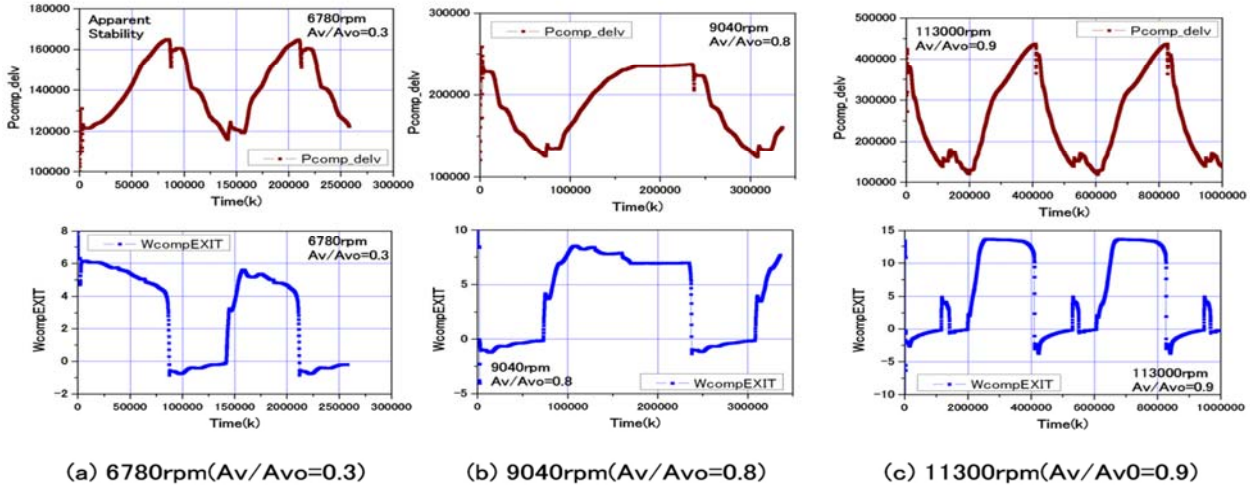

Fig. 7 Transient behaviors of pressures (top figures) and mass flows (bottom figures) at the compressor exit location in deep surge conditions at three compressor speeds.

6. Behaviors of Surge Frequency

Figure 8 shows surge frequencies fs_0 read from the oscillograms for changes in the compressor speeds. It shows a decreasing tendency as a whole for the increasing compressor speeds. The tendency appears to be different above and below the 90 % design speed. The rough tendency is shown by a shaded zone. It includes data for various valve area conditions. Above 10170 rpm, the changes in the valve area ratio from 0.9 to 0.5 are seen to have some small effects on the frequency. The points at and below 9040 rpm are only ones respectively for the first appearance of deep surges during throttling the valve, as shown in **Fig. 5**.

The same data are shown in **Fig. 9** where the surge frequencies fs_0 are plotted against surge pressure ratios *PR*. The surge frequencies appear to be affected also by the surge pressure ratios. It could be interesting to investigate in what a combined manner both the compressor speeds and the pressure ratios could affect the surge frequencies.

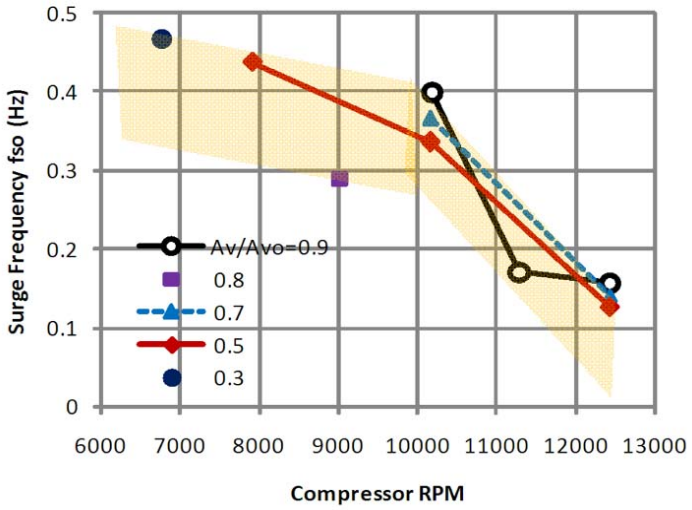

Fig. 8 Surge-cycle frequencies including ones for various valve port areas and a tentative zone

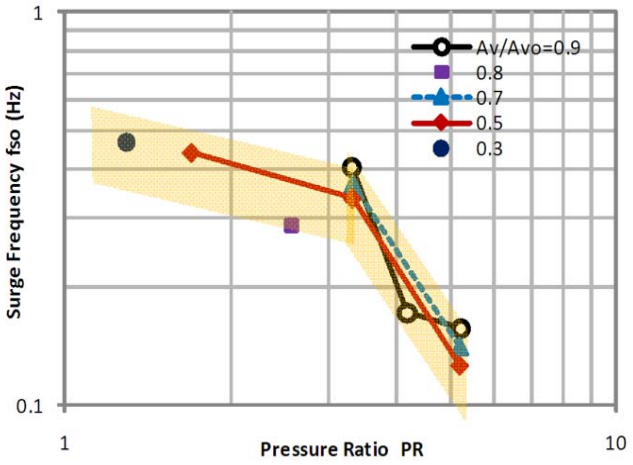

Fig. 9 Effects of compressor stalling pressure ratios on the surge frequencies

7. Mode of Surge Oscillations

Figure 10 shows spatial and temporary maps of transients of typical variables in deep surge conditions. Subfigures are, in the vertical direction, (a) pressure, (b) mass flow, and (c) temperature, and in horizontal direction, (1) 6780 rpm (60% design speed), (2) 10170 rpm (90% design speed), and (3) 11300 rpm (100% design speed). The horizontal axis of each subfigure shows CV locations where the CV numbers are indicated by brown-color letters in **Fig.2**; 1 for the duct inlet, 26-35 for the compressor, 45-70 for the delivery plenum, and 70 for the exit valve. The vertical axis means time *k* upward. Warm colors in **Fig. 10** mean higher values, and cold colors mean lower values, including occasionally negative values.

In the pressure contour maps in **Fig. 10(a)**, pressure changes synchronously over the flow-path downstream of the compressor; the situations are similar for all the compressor speeds. In the mass flow maps in **Fig. 10(b)**, a basic surge phenomenon appears as alternate changes of the reversed flow and the normal flow. Local phenomena of h igher frequency superposed on them appear different, depending on the compressor speeds. In the temperature maps in **Fig. 10(c)**, high temperature contours could serve as tracers for indicating the fluid particle movements and positions. The high temperature contour protruding upstream of the compressor means that the flow particles having once passed through the compressor reversed and reached up to the position in the reversed flow phase. For the higher speed in **Fig. 10(C) (c)**, the fluid is seen to blow back upstream as far as the inlet of the suction duct. On the other hand, for the lower speed in **Fig. 10 (A) (c)**, the fluid is seen to be reciprocating within the narrower range upstream of the compressor. It could be related with the higher surge frequency in the lower compressor speeds. In addition to that, for the higher speed in **Fig. 10 (C)(b)**, a short-term normal flow (insufficient recovery) is seen to intervene in the stalled time-span, resulting in significant variations in the mass flow and the temperature behaviors shown in **Fig.10(C)(b)** and **(c)**.

For reference, **Fig. 11** shows oscillograms at some typical locations, corresponding to the contour maps in **Fig. 10**. Numbers attached to the curves mean CV locations in blue-colored letters in **Fig. 2**, as follows; 12: halfway in the suction duct, 26: immediately upstream of the compressor inlet, 27: immediately downstream of the compressor exit, 37: inlet to the plenum chamber, 45: halfway of the plenum chamber, and 60: the delivery duct exit. The curve behaviors in **Fig. 11** together with the contour maps in **Fig. 10** would help much understanding the situations.

In **Fig. 11 (a) of (A-C)**, small disturbances in the pressure behavior in the suction duct are observed when the mass flow stops and starts as seen in **Fig. 11 (b) of (A-C)**. These are surge hammer-shock pressures in a positive sense and a negative sense, respectively, similar to the water hammer pressures. Smaller oscillations in flow and pressure are excited by the shocks mainly in the suction duct. The phenomena are seen also in the mass flow contours in **Fig. 10 (b) of (A-C)**. The phenomenon has been observed in actual compressors. The oscillations are considered to be of some local resonances, since the frequencies are significantly higher compared with the surge frequency or the whole duct-system resonant frequency, for example, the first resonance frequency, f_1, described in **Section 8**.

Aside from these oscillations, small bulges are seen in the pressure bottom zone for the high-speed data in **Fig. 11 (a) of (C)**. This phenomenon accompanies short-term mass flow recoveries as seen in **Fig. 11(b) of (C)** and **Fig. 10(b) of (C)**. This could be an insufficient recovery from the surge. The insufficient recovery appears to elongate the duration of the reversed flow phase, reducing significantly the surge frequency in the higher compressor speed range such as in **Fig. 8**. One possibility of the cause could be guessed that the duct-system is tending to return to its own fundamental frequency near the first resonance frequency from the present surge frequency that could have been substantially suppressed by the flow convection nature. Regrettably, it is not certain at present whether the phenomenon actually occurs or not, in other words, whether it is a reality or only an analytical phenomenon. Experimental study is required to confirm the results.

The flow transients during surges are seen as above to change much for changes in the compressor speeds. The results above

suggest that various important influential factors and phenomena are involved in the surge; such as, flow-path configurations, acoustical frequencies, compressor tip speed, flow convection effects, pressure ratios, stage mismatching situations, situations of rear stage stalling or front stage stalling, and valve opening area, etc. Many of these factors could affect more significantly the surge behaviors in the multi-stage and high pressure-ratio conditions than in single-stage or few-stage fans of low pressure ratios. Stage characteristics data also could have essential influences on the phenomena, particularly with respect to the reversed flow zone. Valve flow characteristics are also important.

As such, with respect to the details of the surge, it could be said that many phenomena are left unsolved for future study. It requires suitable simulation codes and increases in the accumulation of analytical knowledges and correspondences between the analytical results and the actual data. It might be difficult to construct a simplified model. But it would be necessary and useful to obtain insights into the complicated phenomena and to gain rules of thumb, if possible.

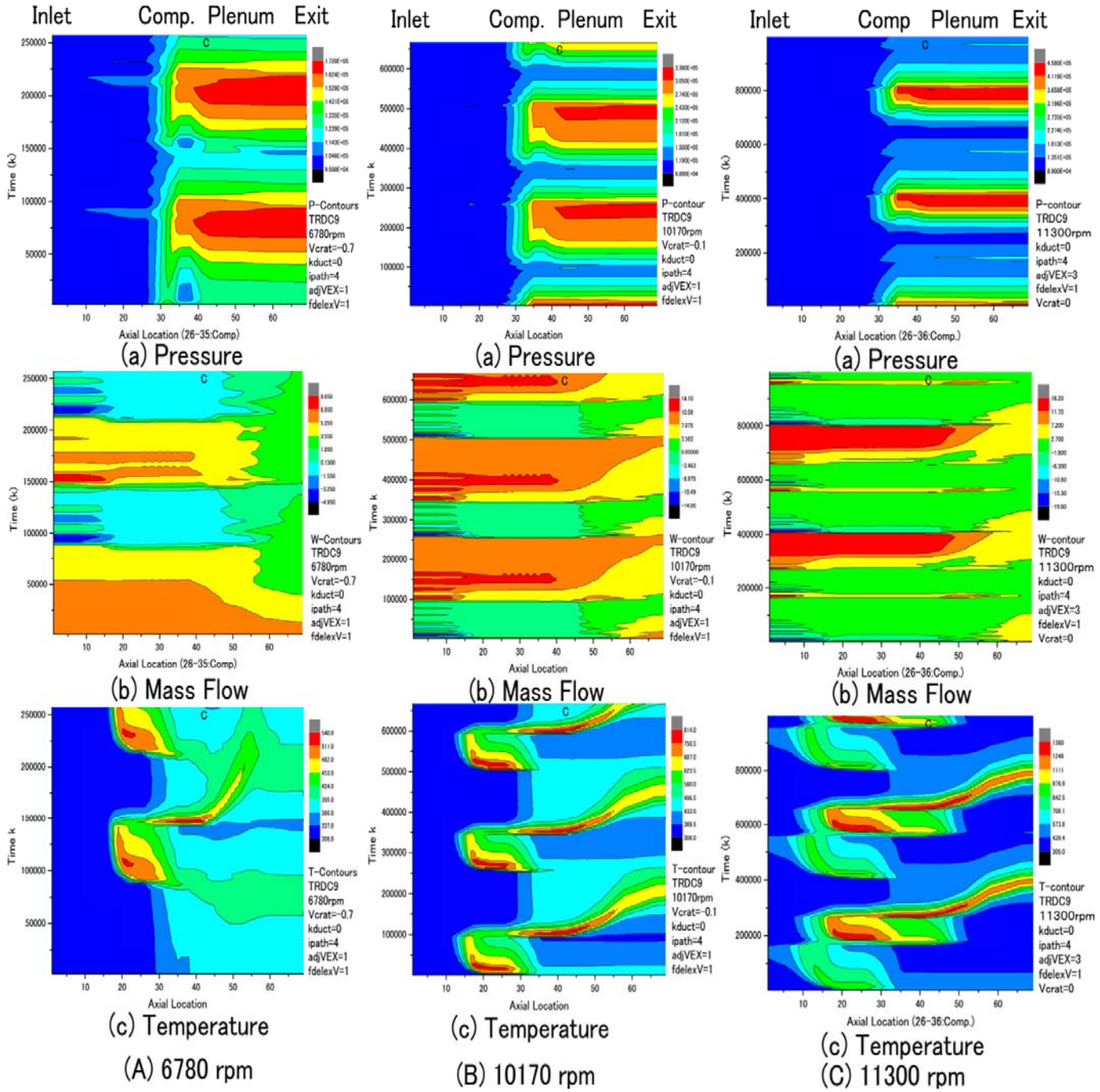

Fig. 10 Comparison of spatial and temporary maps of (a) pressures, (b) mass flows, and (c) temperatures for (A) 6780 rpm, (B) 10170 rpm, and (C) 11300 rpm. Rough positions of the inlet, compressor, plenum, and exit/valve are indicated above the top figures. The compressor exists over from 26 to 35. Time lapses vertically upward in each subfigure. Full time spans are approximately 4, 10, and 14 seconds for (A), (B), and (C), respectively.

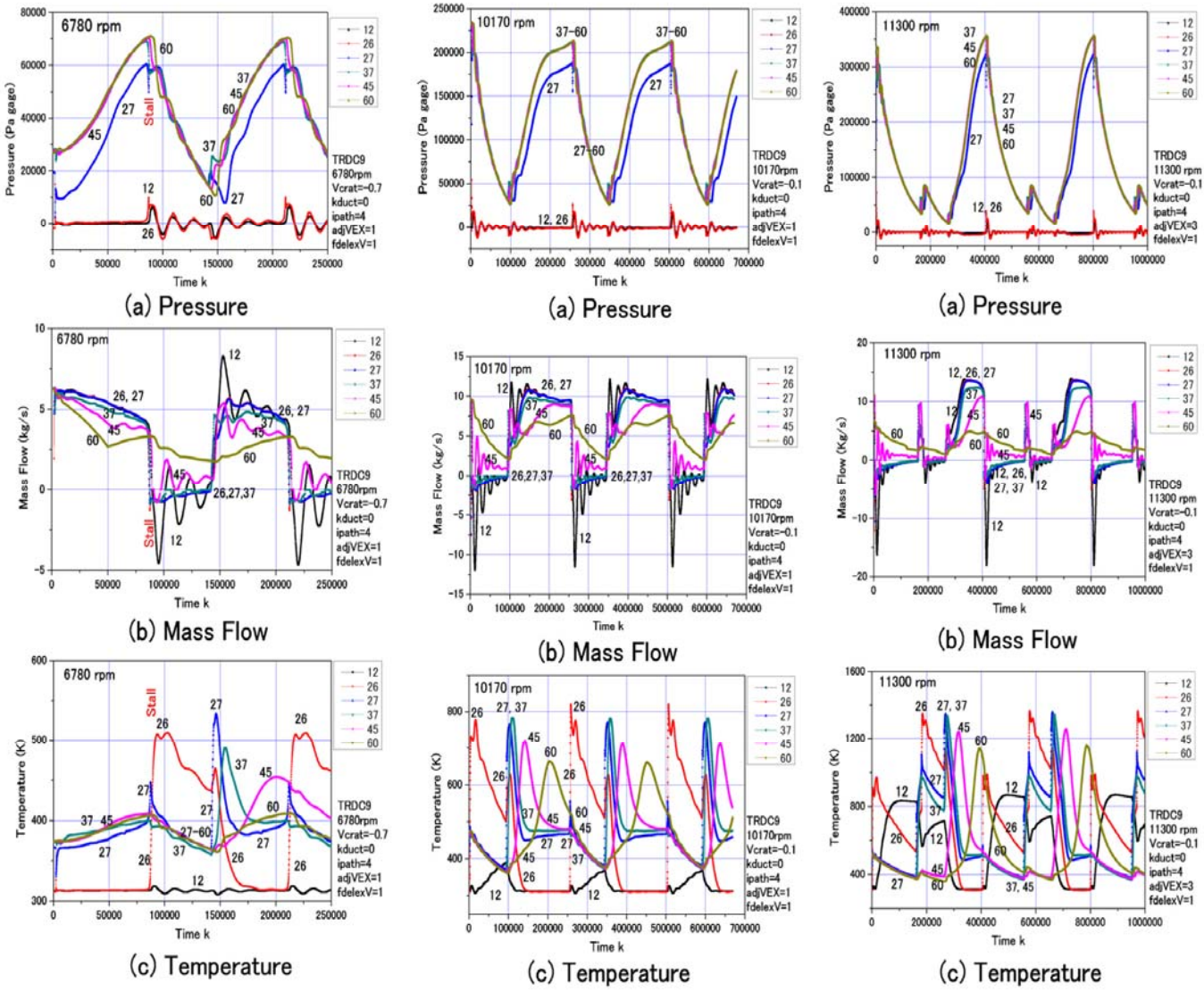

(A) 6780 rpm (B) 10170 rpm (C) 11300 rpm

Fig. 11 Oscillograms of (a) pressure, (b) mass flow, and (c) temperature during surge situations for three speeds. (A) 60% design speed, (B) 90% design speed, and (C) 100% design speed.
Attached numbers show CV locations as follows; 12: halfway in the suction duct, 26: immediately upstream of the compressor inlet, 27: immediately downstream of the compressor exit, 37: inlet to the plenum chamber, 45: halfway of the plenum chamber, and 60: in front of the delivery duct exit.

8. Examinations on the Surge Frequencies

The behaviors of the analytical surge frequencies for changes in the compressor speed obtained here are studied in relation with macroscopic and geometrical parameters.

Figure 12 shows a schematic model together with the typical sizes of the compressor- duct system. The delivery flow-path modeled as a plenum has a sectional area *Ap* and a length *Lp*. The suction flow-path including the compressor is modeled as to have a representative length *Lc*** from the duct inlet to the compressor exit and a representative sectional area Ac_2 of the exit area of the last stage of the compressor.

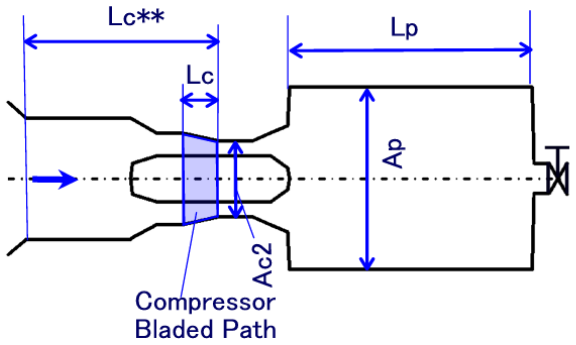

Fig. 12 Typical dimensions for expressing the compressor -duct system

(1) Surge frequencies and reference frequencies

Figure 13 compares the surge frequencies fs_0, the first

resonance frequencies $f_1$of the duct system, and Helmholtz resonator frequencies *fo* against the compressor speeds.

The first resonance frequency f_1 of the air column in the whole flow-path is paid attention to as the basic frequency in the system. It is evaluated by the acoustical differential equation as an acoustical resonance frequency in the still air in the whole duct system with an open-end inlet and a closed-end exit. In the evaluation, the temperature distributions are specified on the basis of the flow-path data before stalling, and the pressures are kept constant at the atmospheric one throughout the flow-path system.

The Helmholtz resonator frequency *fo* is often employed in surge consideration (for example, Greitzer [6]). It is an approximation to f_1 in a duct having a Helmholtz resonator configuration approximated here as constructed by an inlet pipe with the sectional area Ac_2 and length Lc^{**} and a plenum chamber with the volume Vp (=$ApLp$).

$$f_0 = \frac{a}{2\pi}\sqrt{\frac{A_{c2}}{V_P L_C^{**}}} \qquad (10)$$

Here, a is the average speed of sound. The accuracy of f_0 is affected by the relative length to the wave length. In a duct system having a rather complicated configuration, the accuracy could be affected significantly by the arbitrariness in the choice of the representative sizes.

In **Fig. 13**, the basic frequency f_1 given by a black dotted line shows a nearly constant value over the compressor speeds. The Helmholtz frequency f_0 here is given by a blue one-dot- chain line running below f_1 in a parallel fashion. Both f_1 and f_0 are little affected by the compressor speeds because of the simple resonance nature in the duct system. Here, f_1 is the more reasonable reference frequency.

The surge frequency fs_0 is lower than f_1 and lessens further toward the higher-speed region. The observed large discrepancy and different behaviors between the surge frequencies fs_0 and the first resonance frequencies f_1 are intensely interested in.

For reference, the data points below 10000rpm are for the valve opening of the first appearance of deep surge conditions during throttling the valve by 10%. An example of the situation was shown in **Fig. 5**. Above 10000 rpm, the frequency data given here are for the valve area ratios of 90% and less.

The red dotted-line shows an fs_0 behavior predicted by Eq. (17) described later for reference. It is seen to give a rough tendency of the behavior as a whole against the compressor speeds.

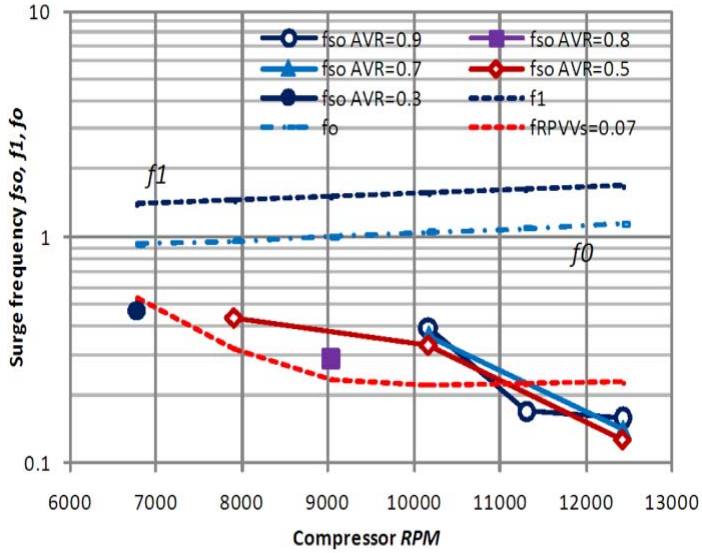

Fig. 13 Behavior of predicted surge frequencies against compressor speeds compared with the first resonance frequencies, etc.

(2) Reduced surge frequencies

From the aspect of flow-induced oscillation, attention is paid to reduced surge frequencies, which will be defined as follows;

$$f_{RPs}=Lpfs_0/u_t \qquad (11)$$

$$f_{RCs}=Lc^{**}fs_0/u_t \qquad (12)$$

The delivery plenum length Lp and the compressor-suction duct length Lc^{**} are employed as the representative lengths. Rotor tip speed u_t is used as the representative speed.

Figure 14 shows behaviors of both reduced surge frequencies against the compressor speeds. These reduced frequencies are seen to drop fairly steeply with an increase in the compressor speed. It is suggested that f_{RPs} could dominate the surge phenomena in this particular case, since f_{RPs} is seen to be much larger than f_{RCs}. But no further information could be found here.

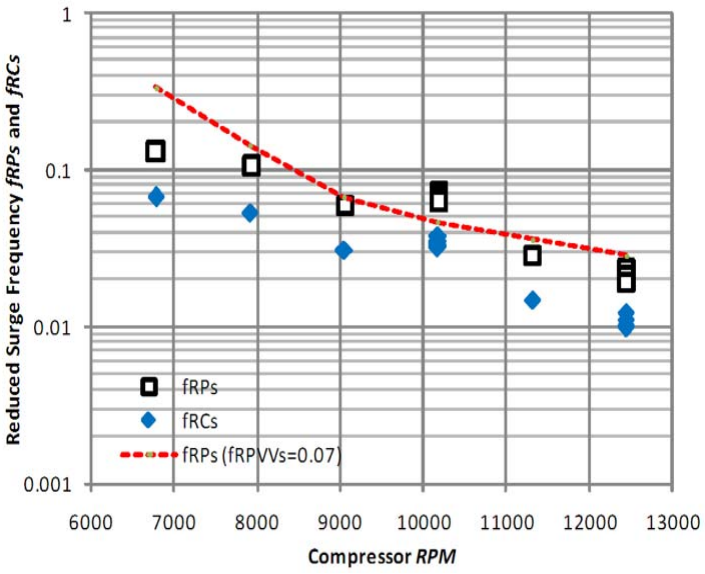

Fig. 14 Changing reduced surge frequencies against compressor speeds

The red dotted-line shows an f_{RPs} behavior predicted by Eq. (18) described later for reference. It is seen to give the tendency rather well.

(3) Corrected reduced surge frequency

By taking a ratio of the compressor mass flow into the delivery plenum in one surge period, Eq. (13) below, and the increase in the air mass stored in the plenum, Eq. (14) below, the following dimensionless quantity f_{RPVs} is derived. Here, a density ratio is assumed to be given by an isentropic change in relation with the pressure ratio.

Compressor delivery mass in one surge period: $A_{C2}u_t PR^{1/\kappa} / f_{S0}$ (13)

Increase in the mass stored in the plenum: $V_P(PR^{1/\kappa} - 1)$ (14)

$$f_{RPVVs} = \frac{f_{S0}V_P(PR^{1/\kappa}-1)}{A_{C2}u_t PR^{1/\kappa}} = \frac{f_{S0}L_P(1-PR^{-1/\kappa})}{u_t}\frac{A_P}{A_{C2}} = f_{RPs}\frac{A_P}{A_{C2}}(1-PR^{-1/\kappa}) \quad (15)$$

The non-dimensional parameter f_{RPVVs} is named here "volume-modified reduced surge frequency", since it is related to the plenum reduced surge frequency f_{RPs} as above. Values of f_{RPVVs}, estimated from the data in **Figs. 8** and **9**, are shown in **Fig. 15**. The pressure ratios *PR* used in the evaluations are corresponding to the respective initial stalling values.

In comparison with the ordinary reduced surge frequencies f_{RPs} given in **Fig. 14**, the volume-modified reduced surge frequencies f_{RPVVs} show nearly the same level over the low speed range, although they show a somewhat lowered level in the high speed range. From the observation, as far as this system is concerned, the averaged level of the volume-modified reduced surge frequencies could be given very approximately as follows;

$$f_{RPVVs} \sim 0.07 \quad (16)$$

The constant level of the volume-modified reduced surge frequency may be considered to reconfirm the surge mechanism as the process of emptying and filling the air in the plenum.

When the value of f_{RPVVs} is specified, the surge frequency and the reduced surge frequency could be determined by the following relations.

$$f_{S0} = f_{RPVVs}\frac{u_t}{1-PR^{-1/\kappa}}\frac{A_{C2}}{A_P L_P} \quad (17)$$

$$f_{RPs} = f_{RPVVs}\frac{1}{1-PR^{-1/\kappa}}\frac{A_{C2}}{A_P} \quad (18)$$

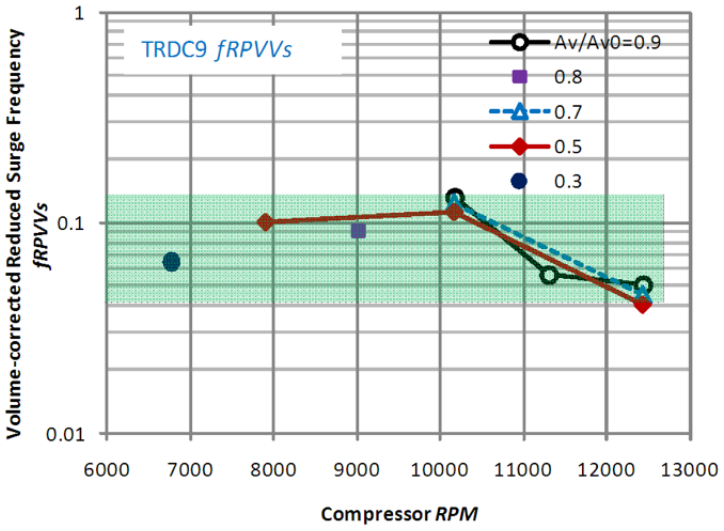

Fig. 15 Volume-modified reduced surge frequencies vs. compressor rpm

The surge frequencies *fso* and the reduced surge frequencies f_{RPs} thus evaluated by Eqs. (17) and (18) are inserted as red dotted-lines in **Figs. 13** and **14**, which are seen to show the tendencies of the behaviors roughly well.

It is understood that both the compressor speeds u_t and the compressor pressure ratios *PR* are finally combined as in Eq. (17) to give the surge frequency behavior.

Since the values of f_{RPVVs} appear somewhat changeable depending on the flow-path configurations, the compressor operating conditions, such as tip speeds, etc., more case studies and experimental studies will be required.

(4) Duration time by reversed flow phase in surge

The behavior of the surge frequencies show some ups and downs against compressor speeds. In relation with the behaviors, times occupied by the reversed flow phase and the normal flow phase in a surge cycle were read from the related oscillograms at the exit of the compressor, such as in **Fig.7** and **Fig. 11(b)**. **Figure 16** shows the respective times of the reversed flow phase $T_{s\text{-}rev}$ and the normal flow phase $T_{s\text{-}normal}$ and the total surge cycle T_{so} at the compressor exit against the compressor speeds. The normal flow phase time $T_{s\text{-}normal}$ shows a relatively smoothly increasing tendency with increasing compressor speed. The reversed flow phase time $T_{s\text{-}rev}$ shows some gap in the levels between for the lower speeds and for the higher speeds. The total cycle time T_{so}, a sum of the two, results in the unsmooth distribution.

Reduced surge times τ_S are evaluated from the surge times in an analogous manner to the above reduced frequency. Here, $\tau_{s\text{-}rev}$, $\tau_{s\text{-}normal}$, and τ_{so} are corresponding to $T_{s\text{-}rev}$, $T_{s\text{-}normal}$, and T_{so}, respectively. The reference speed uses the compressor axial velocity at stall ($u_t \phi_{stall}$) where ϕ_{stall} is the stage stalling flow coefficient.

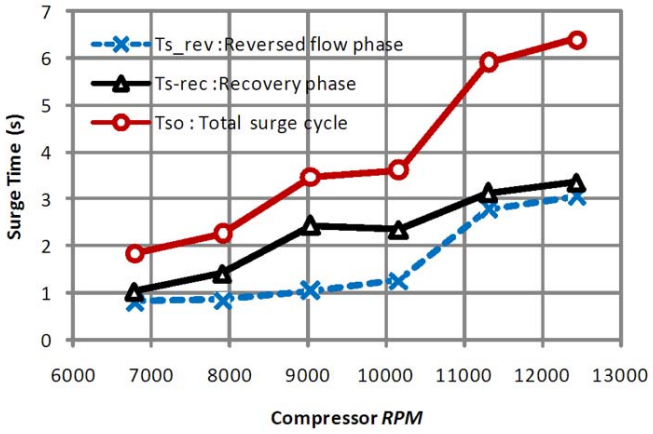

Fig. 16 Surge time period of recovery flow, reversed flow and total surge period

$$\tau_{S0} = \frac{T_{s0} u_t \phi_{stall}}{L_P \left(1 - PR^{-1/\kappa}\right)} \frac{A_{C2}}{A_P} \quad (19a)$$

$$\tau_{S-rev} = \frac{T_{s-rev} u_t \phi_{stall}}{L_P \left(1 - PR^{-1/\kappa}\right)} \frac{A_{C2}}{A_P} \quad (19b)$$

$$\tau_{S-normal} = \frac{T_{s-rec} u_t \phi_{stall}}{L_P \left(1 - PR^{-1/\kappa}\right)} \frac{A_{C2}}{A_P} \quad (19c)$$

In the equations above, $(u_t \phi_{stall})(Ac2/Ap)$ means the axial velocity in the plenum at the compressor stage stalling.

Figure 17 shows the distribution of the reduced surge times against compressor speeds. Here the value of ϕ_{stall} is set equal to 0.3. It is seen that both $\tau_{s\text{-normal}}$ and $\tau_{s\text{-rev}}$ have the same order of magnitude near unity, which suggests again that the surge is a phenomenon of emptying and filling the plenum. The reduced time of the filling phase, $\tau_{s\text{-normal}}$, behaves relatively smoothly against the compressor speed. But the reduced time of the emptying phase, $\tau_{s\text{-rev}}$, shows an abrupt increase in a discontinuous manner. The larger values of $\tau_{s\text{-rev}}$ in the high speed zone could be related with the appearance of the insufficient recovery phenomenon, whose intervention as seen in **Fig. 10 (C)(b)** could have elongated the reversed flow time, resulting in the reduction of the surge frequency.

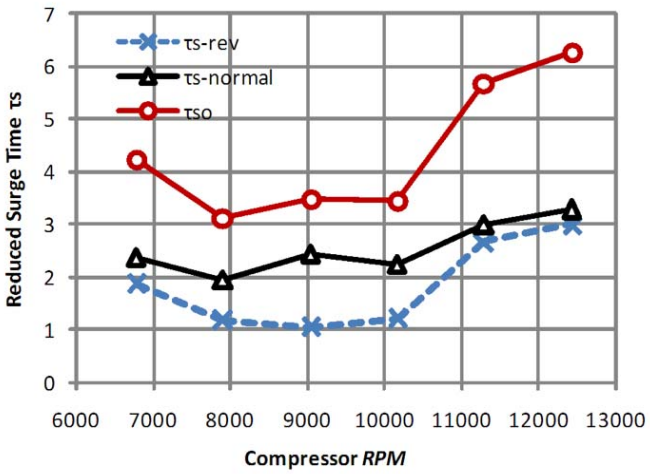

Fig. 17 Reduced surge time period of recovery flow, reversed flow and total surge period

The results could suggest also the working conditions of the rear stages of the compressor since the location of the data acquisition is at the compressor exit. The behaviors of the surge times in **Figs. 16** and **17** could suggest some differences in the tendency above and below 10170 rpm (90% design speed) in addition to the frequency tendencies given in **Figs. 8, 9** and **13**. It could possibly reflect the differences in the stage working situations between in the front stage stalling condition in the lower speed region and in the rear-stage stalling condition in the higher speed region.

9. Positioning relative to the Stall Stagnation Boundary

The surge phenomena should be examined in relation with the stall stagnation boundary, which is the limiting condition beyond which the stall behaviors no longer show deep surges but fall into the rotating stall branch of the characteristics. The compressor tends to stagnate in the dangerous situation. In jet engines, it is often called "hung stall" or "non-recoverable stall". The details of the boundaries are described in Yamaguchi [2, 3].

Figure 18 shows the acoustical and geometrical stall stagnation boundary given by Yamaguchi [2, 3], which shows the boundary for vanishing of deep surges. In **Fig. 18**, the following normalized parameters are employed.

Relative plenum length:

$$RLP = Lp/\lambda \quad (20)$$

Relative compressor-duct length:

$$RLC = Lc^{**}/\lambda \quad (21)$$

Plenum area-pressure ratio:

$$APR = (Ap/Ac_2)PR \quad (22)$$

Here,

$\lambda = a/f_1$: acoustic wavelength of the first resonance frequency in the whole flow-path system, and

a: average sound of speed in the whole flow-path.

Other variables were explained earlier in relation with **Fig. 12**.

Legend in **Fig. 17**, for example," RL_stg_9_10000_0.9" means *RLP* and *RLC* for the condition of a nine stage compressor, 10000rpm, and valve area ratio of 0.9. "APR_stg_9_10000_0.9" means *APR* for the same condition. Here, data for the nine-stage compressor (marks ○ and △) are paid attention to, although **Fig. 18** includes data for a single stage compressor also (colored marks). Curves connecting the points are the stall stagnation boundary and the yellow shaded zones bounded by the curves indicate the zone of deep surge occurrence. Typical two boundaries, B and A, and an intermediate one, form the stagnation boundary.

The stall stagnation boundary changes widely for changes in the configurations of the flow-path system and the compressor conditions. The B-boundary shows the one for delivery duct having a short-and-fat plenum configuration. It is corresponding roughly to the limiting condition given by a specified value of Greitzer's B parameter (Greitzer [6]). The A-boundary shows similar conditions for long and narrow delivery ducts. As seen in **Fig.18**, at B- boundary for sufficiently small values of *RLP*, *RLC* has a value of nearly 0.25 and *APR* increases toward smaller *RLP*. At A- boundary for sufficiently small values of *RLC*, *RLP* has a value of nearly 0.2 and *APR* has a value of nearly 2.

The conditions of the compressor-duct system for the present study are shown in **Fig. 18** by points of + and × marks named "TRDC9". The system is seen to be located within the deep-surge zone of the nine-stage compressor. The points of (*RLP, RLP*) move only slightly for the speed changes, but the *APR* points are seen to approach the A-boundary for the reducing compressor speeds. It is seen that the present case has not reached the stall stagnation boundary, but come

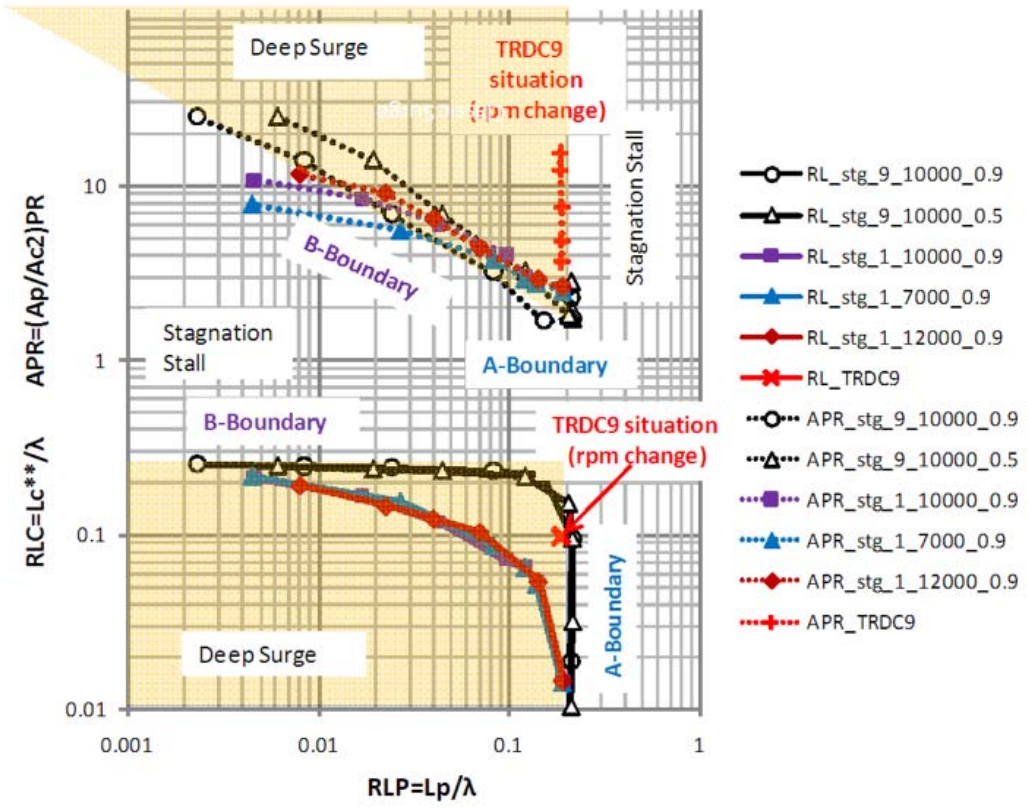

Fig. 18 Working situations of the present compressor-duct system relative to the geometrical stall-stagnation boundaries (Yamaguchi [2,3])

near the boundary in the lower speed zone. It is not certain at present whether the situation could have any relationship with the predicted appearance of the apparently stable non-surge area.

10. Significance of the Area-Pressure Ratio

The area-pressure ratio parameter *APR* for the stall stagnation boundary had been found intuitively by looking over the tendency of the sectional area data in the first place (Yamaguchi [2, 3]). The significance, which was rather ambiguous then, has now become somewhat clearer on the basis of Eq. (15) found in this study. At the same time, the behavior of the *APR* vs. *RLP* for the stall stagnation boundary shown in the upper zone of **Fig. 18** could be explained qualitatively.

Equation (15) is transformed as follows.

$$APR \equiv (\frac{A_P}{A_{C2}})PR = \frac{f_{RPVVs}}{f_{RPs}} G(PR) \tag{23}$$

Here, $G(PR)$ means the following function of the pressure ratio PR.

$$G(PR) = \frac{PR}{1 - PR^{-1/\kappa}} \tag{24}$$

If, at the stagnation stall boundary, Eqs. (23) and (24) is assumed to be valid and the volume- modified reduced surge frequency f_{RPVVs} is assumed to have some constant value, then the area- pressure ratio *APR* at the stagnation boundary is inversely proportional to the reduced surge frequency f_{RPs}. The function $G(PR)$ has values changing gradually from approximately 5 to 7 for the value of *PR* from 2 to 5.

For example, let us conduct a trial calculation as follows. Set temporarily

PR=3, G(PR)~5.5 and f_{RPVVs}=0.07.

The above value of f_{RPVVs} was assumed as a tentative one. Some inspections on f_{RPVVs} values showed smaller values changing gradually along the stagnation boundary.

At A-boundary, the limiting reduced surge frequency f_{RPs} tends to be about 0.2 (Yamaguchi [2, 3]), and the following value is obtained from Eq. (23).

APR~1.9.

At B-boundary, the limiting reduced surge frequency f_{RCs} and the relative length *RLC*=*Lc***/λ tend to be 0.2 and 0.25, respectively (Yamaguchi [2, 3]). From Eqs. (10) and (11), f_{RPs} is estimated as follows;

$f_{RPs}=f_{RCs}$ (Lp/Lc^{**}) ~0.2 (Lp/Lc^{**}) =0.2 (RLP) / (RLC) for the B-boundary

which yields

f_{RPs}~0.8(RLP) for the B-boundary.

For example, at RLP =0.1and 0.01 for the B-boundary, the values of f_{RPs} are estimated as follows;

f_{RPs} = 0.08 and 0.008, respectively.

Then, the following respective values are obtained from Eq. (23).

APR~ 4.8 and 48 for RLP =0.1and 0.01, respectively.

These estimated values for both the A- and B- boundaries could explain very roughly the behavior of APR vs. RLP along from the A-boundary to the B-boundary in **Fig. 18**, though not in very good agreement at present. With respect to the APR behaviors, further detailed information is desired in relation with the volume-modified reduced surge frequency f_{RPVVs} on the basis of more case studies and examinations.

The above very rough evaluations suggest that the area-pressure ratio parameter APR means the dynamic condition related with the surge frequency, compatible with the flow convection process of filling and emptying of gas into and out of the delivery flow-path. On the other hand, the boundary for RLC vs. RLP is the limiting condition with respect to the possibility of continued self-excitation compatible with the acoustical mode existing in the flow- path, as has been given in Yamaguchi [2, 3].

11. Extended Pressure-Flow Area in the Low-Speed Zone

In **Sections 5** and **6**, apparently workable area extended far over the initial stage-stalling line was calculated in the lower speed zone in the course of throttling the valve. The area is a non-surge, globally stable but locally unstable one, often referred to as rotating stall zone in conventional performance maps of high-pressure ratio compressors (for example, Ref. [7]). It is seemingly a stable zone, but a very dangerous one if the compressor stays there long. It is required to pass through the zone quickly during the start-up or the shut-down.

With respect to the phenomenon of light stalling and instantaneous recovery shown in **Fig. 5(e)**, no actual experiences have been known to the author. As far as the analysis is concerned, it might be ascribed to the presence of the discontinuity in the pressure coefficient behavior at stall in the stage characteristics shown in **Fig. 1**. Stage stalling behaviors for lower speeds or lower Reynolds number conditions could become milder one. If it had a smoother or milder stalling characteristics, the light stalling phenomena in the multi-stage compressor might not have appeared in the analysis.

The lower-speed tendency in surge line predicted by SRGTRAN as in **Fig. 5** suggests the validity of the method to a certain extent. However, it will be required that the data on the stage characteristics including the stage stalling manner should be more accurate for more realistic simulation. In this concern, the author wishes to try various configurations of the stage characteristics to study the effects on the overall compressor performances.

12. Conclusion

Surge phenomena in the zone of reduced speeds in a nine-stage axial flow compressor were studied analytically by use of a surge transient simulation program of own coding, SRGTRAN. Several interesting findings were obtained with respect to the low-speed surge behaviors. At the same time, several tasks have also been found. Main results are summarized as follows.

(1) A significant expansion of apparently stable non-surge area in the pressure-flow map beyond the initial stage-stall line was analytically predicted in the lower speed region. The predictability of the zone, which has conventionally been observed in actual multi-stage machines, suggests the validity of the code in a sense. The zone is, in fact, very dangerous owing to the presence of rotating stalls in front stages.

(2) Surge frequencies were found to increase for decreasing speeds as far as the particular compressor was concerned.

(3) A new parameter of volume-modified reduced surge frequency was introduced to explain the tendency. It is seen to be kept at nearly the same level over the analyzed compressor speeds. It suggests that the surge is, as is known, essentially of flow convection nature and the frequency is determined by the process of emptying and filling of gas into the delivery volume.

(4)The area-pressure ratio parameter in the stall stagnation boundary, proposed earlier by the author (Yamaguchi [2, 3]), was found to be tentatively explained on the assumption of the constancy of the volume-modified reduced surge frequency.

(5)Several phenomena observed here, such as the insufficient surge recovery, the lightly stalling and instantaneous recovery, the area-pressure parameter in the stall stagnation boundary, and the discrepancy between the surge frequency and the acoustical resonance frequency, etc. are tasks for further study needing confirmation including whether they are reality or only analytical one. In addition to that, some of the various differences observed among the surge phenomena for changing compressor speeds require also further study for clarification of the whole picture of the complicated surge phenomena, and for putting together into simpler forms, if possible.

The results are all based on the analytical data by SRGTRAN. There remain many items left for future study including experimental confirmations and verifications.

The author would be happy if the content of this paper could be of some help to the readers.

Nomenclature

a	Speed of sound (m/s)
$Ac2$	Sectional area of the exit of the compressor last stage (m^2)
APR	Area –pressure parameter
Av	Valve opening area (m^2)
Avo	Initial valve opening area immediately before steady stalling (m^2)
Cp	Specific heat at constant pressure (J/kg/K)
f_0	Resonance frequency of a Helmholtz resonator (Hz)
f_1	The first resonance frequency of an air column (Hz)
f_{RCs}	Reduced surge frequency with respect to the suction duct
f_{RPs}	Reduced surge frequency with respect to the delivery (plenum) duct
f_{RPVVs}	Volume-modified reduced surge frequency
f_{s0}	Surge frequency (Hz)
$G(PR)$	Function of PR
k	Time integer
Lc^{**}	Length of the compressor-suction flow-path (m)
L_P	Length of the delivery (plenum) flow-path (m)
PR	Pressure ratio
Ps	Surge pressure (Pa, Pa G)
RLC	Relative length of the compressor-suction flow-path
RLP	Relative length of the delivery (plenum) flow-path
t	Time (s)
Ts	Flow temperature（K）, or Surge cycle time (s)
T_{S0}	Surge cycle time(s)
$T_{S\text{-}normal}$	Normal flow time during surge (s)
$T_{S\text{-}rev}$	Reversed flow time during surge (s)
u_m	Annulus-averaged axial flow speed (m/s)
u_t	Referential blade tip peripheral speed (m/s)
$Vcrat$	Rate of valve opening change
Vp	Delivery plenum volume (m^3)
W	Mass flow (kg/s)
Wv	Valve mass flow (kg/s)
x	Axial coordinate along the flow-path (m)
αv	Valve flow coefficient
βv	Valve flow adjusting coefficient
ΔLv	Equivalent length of valve passage (m)
Δt	Time step (s/div)
κ	Ratio of specific heats
λ	Wave length for f_1 (m)
ρ	Flow density (kg/m^3)
φ_t	Stage flow coefficient
ψ_{Pt}	Stage pressure coefficient
ψ_{Tt}	Stage temperature coefficient
τ_{s0}	Reduced surge time corresponding to Tso
$\tau_{s\text{-}normal}$	Reduced surge time corresponding to $Ts\text{-}normal$
$\tau_{s\text{-}rev}$	Reduced surge time corresponding to $Ts\text{-}rev$
εv	Coefficient of valve passage length

Suffices

s-norm	Time for normal flow in surge
s-rev	Time for reversed flow in surge
S	Static condition
T	Total condition
v	Valve

References

[1] Yamaguchi, N., 2013, Development of a Simulation Method of Surge Transient Flow Phenomena in a Multistage Axial Flow Compressor and Duct System**,** International Journal of Fluid Machinery and Systems, Vol. 6, No.4, pp. 189-199

[2] Yamaguchi, N., 2012, A Study on the Stagnation-Stall Boundaries Based on Analytically-Evaluated Surge Conditions in Axial Flow Compressors, No. ISUAAAT13-S5-1, The 13-th International Symposium on Unsteady Aerodynamics, Aeroacoustics and Aeroelasticity of Turbomachines,

[3] Yamaguchi, N., 2013, Analytical Study on Stall Stagnation Boundaries in Axial-Flow Compressor and Duct Systems, International Journal of Fluid Machinery and Systems, Vol. 6, No. 2, pp. 56-74

[4] Day, I. J. , Greitzer, E. M., and Cumpsty, N. A., 1978, Prediction of Compressor Performances in Rotating Stall, Trans. ASME, Jour. of Eng. for Power, Vol.100, No.1, pp. 1-14

[5] Gamache, R.N. and Greitzer, E.M., 1986, Reverse Flow in Multistage Axial Compressors, AIAA -86 -1747

[6] Greitzer, E.M., 1975, Surge and Rotating Stall in Axial Flow Compressors, Part II: Experimental Results and Comparison with Theory, ASME paper, 75-GT-10

[7] Handbook of Air and Gas Machinery (editor: Hatta, K.), Section 2.2, Axial Flow Fans and Compressors (in Japanese), Asakura Publishing Co. (1969), pp. 295